Journal of Molecular Graphics and Modelling 61 (2015) 133–140

Contents lists available at ScienceDirect

Journal of Molecular Graphics and Modelling

journal homepage: www.elsevier.com/locate/JMGM

Andrographolide: A potent antituberculosis compound that targets Aminoglycoside 2′-*N*-acetyltransferase in *Mycobacterium tuberculosis*

Amudha Prabu[a], Sameer Hassan[b], Prabuseenivasan[a], Shainaba A.S.[a], Hanna L.E.[b], Vanaja Kumar[c,*]

[a] Department of Bacteriology, National Institute for Research in Tuberculosis, Chetpet, Chennai 600031, India
[b] Department of Biomedical Informatics, National Institute for Research in Tuberculosis, Chetpet, Chennai 600031, India
[c] Centre for Drug Discovery and Development, Sathyabama University, Chennai 600119, India

ARTICLE INFO

Article history:
Received 10 April 2015
Received in revised form 13 July 2015
Accepted 14 July 2015
Available online 21 July 2015

Key words:
Tuberculosis
Antimycobacterial activity
Andrographolide
Drug target
Docking
Molecular simulation

ABSTRACT

Tuberculosis (TB) still remains a major challenging infectious disease. The increased rate of emergence of multi-drug resistant and extensively-drug resistant strains of the organism has further complicated the situation, resulting in an urgent need for new anti-TB drugs. Antimycobacterial activity of *Andrographis paniculata* was evaluated using a rapid LRP assay and the probable targets were identified by docking analysis. The methanolic extract of *A. paniculata* showed maximum antimycobacterial activity at 250 μg/ml against all the tested strains of *M. tuberculosis* (H37Rv, MDR, and drug sensitive). Based on bioassay guided fractionation, andrographolide was identified as the potent molecule. With the docking analysis, both ICDH (Isocitrate Dehydrogenase) and AAC (Aminoglycoside 2′-*N*-acetyltransferase) were predicted as targets of andrographolide in *M. tuberculosis.* Molecular simulation revealed that, ICDH showed low binding affinity to andrographolide. However, for AAC, the andrographolide was observed to be well within the active site after 10 ns of molecular simulation. This suggests that ACC (PDB ID 1M4I) could be the probable target for andrographolide.

1. Introduction

Tuberculosis (TB) is one of the world's oldest and most challenging infectious diseases. It is the second leading cause of death from a single infectious agent, after human immunodeficiency virus (HIV) [1]. In the year 2013, WHO estimated that 11 million people developed TB and 1.5 million died from the disease, of which 3,60,000 were HIV-positive [2]. The risk of developing TB is also higher in persons with diabetes and other chronic debilitating diseases associated with immune compromise. Even though TB is a curable disease, it requires lengthy treatment extending up to a period of six months or more, with a cocktail of drugs with lots of side effects. Due to the rampant use of anti-tuberculosis drugs, there is an increasing emergence of resistant, not only to the front-line drugs isoniazid and rifampicin, but also to an increasing number of second-line drugs, giving rise to multi drug resistant (MDR) strains and extensively drug resistant (XDR) strains [3,4]. This situation brings us face-to-face with the urgent need for developing new drugs that are more potent, and also new regimens that can shorten the time of treatment, are inexpensive, safe, capable of tackling resistant strains and be used for providing effective treatment for non-replicative latent forms without interfering with antiretroviral therapy. Since the introduction of Rifampicin over 50 years ago, most TB drugs that have been developed are new formulations of existing agents [5]. In the present study, the bioactive compound isolated from a natural source was screened for activity against *Mycobacterium tuberculosis*.

Dating back to the Vedic period, usage of plants and other natural products has remained a template for the development of new scaffolds of drugs [6]. According to the World Health Organization, over 80% of the world's population relies on traditional plant-based systems [7]. The primary benefits of using plant derived medicines are that they are relatively safer than synthetic derivatives, offer profound therapeutic benefits and are more affordable. India is one of the few countries in the world which has a unique wealth of medicinal plants and vast traditional knowledge on the use of herbal medicines for cure of various diseases [8]. Gautam et al. [9] reviewed the anti-mycobacterial activity of certain plant families like *Asteraceae, Fabaceae* and *Apiaceae.* When compared to the rich biodiversity and ethanomedicinal knowledge available in India, only a few plants have been evaluated for ativity against mycobacteria.

* Corresponding author.
E-mail address: vanaja_kumar51@yahoo.co.in (V. Kumar).

http://dx.doi.org/10.1016/j.jmgm.2015.07.001
1093-3263/

Andrographis paniculata commonly known as "King of bitters" has been effectively used in traditional Asian medicine for centuries as an immune booster. *A. paniculata* has properties of immense value such as immune-stimulatory, anti-inflammatory, anti-fertility, liver protection, anti-HIV activity and bile secretion stimulating agent [10,11]. Although *A. paniculata* exhibits various biological activities, much work has not been carried out to examine its activity against clinical isolates of *M. tuberculosis.* Hence, in the present study, the antimycobacterial activity of *A. paniculata* was evaluated using LRP assay, and probable targets were identified by docking analysis.

2. Materials and methods

2.1. Plant collection and Preparation of plant extract

A. paniculata was collected from Virudhunagar district, Tamil Nadu, India. The collected plant material was identified by a taxonomist and it was shade dried at room temperature. The dried material was powdered using an electric blender and it was sequentially extracted with solvents such as hexane and methanol (1:5) using soxhlet apparatus [12]. After complete extraction, the extract was filtered using filter paper (Watmann No. 1) and condensed to obtain solvent free residue and it was stored at −20 °C until use. Stock solution of extract at 1000 μg/ml was prepared with DMSO (final concentration of 1% v/v) from which two working concentrations (250 and 500 μg/ml) were prepared for testing of anti-mycobacterial activity.

2.2. Antimycobacterial activity by LRP assay

Antimycobacterial activity of *A. paniculata* was evaluated against two strains of *M. tuberculosis*—a drug-resistant strain (resistant to first line anti-TB drugs like streptomycin, isoniazid, rifampicin, ethambutol) and a drug-susceptible clinical isolate, along with the reference strain, *M. tuberculosis* H_{37}Rv, following the standard protocol [13]. A uniform thick suspension of *M. tuberculosis* equivalent to # 2 Mc Farland standards was prepared in G7H9 broth. For each sample, 2 drug-free controls and duplicate tests at the specified drug concentrations were set up. Hundred microliters of the suspension was added to 400 μl of 7H9 with and without test compound. Rifampicin (2 μg/ml) was included as the reference control. Cultures were incubated for 72 h. After incubation, 50 μl of high titre phage phAE129 was added. After 4 h of incubation, 100 μl of D-luciferin reagent was added to an equal volume of the phage-cell mixture and the relative light units (RLU) was measured in a Luminometer (Monolight 2010) at 10 s integration time. The percentage reduction in RLU was calculated in comparison to the drug free control and the activity was determined.

2.3. Isolation of active compound

After confirming the activity, the crude methanol extract of *A. paniculata* was fractionated using silica gel column chromatography with gradient elution of Chloroform and Methanol (10% increment with Methanol). Six major fractions were obtained based on similarities in TLC profiles [11]. A potent active principle was identified based on bioassay-guided fractionation. Purity of the active fraction in the crude extract was confirmed with HPTLC. Structural identification of active isolate was based on spectral analysis (^{1}H and ^{13}C NMR, UV and FT-IR).

2.4. Preparation of protein structures and ligands for docking

The crystal structures of known drug target proteins in complex with cognate ligands were downloaded and prepared using Discovery Studio V2.0. The protonation state of the charged residues in the protein structures was done using the GOLD (Genetic Optimization for Ligand Docking, version 5.2) software [14]. The structure of andrographolide (CID 5318517) was downloaded from PubChem database [15]. Protonation state of andrographolide was generated corresponding to an aqueous environment at pH 7.4, i.e. hydrogens were added in the appropriate position using GOLD software.

2.5. Molecular docking analysis

The probable active site for the selected protein structures were identified based on the bound cognate ligand in the available crystal structure. Wherever there was no protein cognate complex, the structure was superimposed with homologous structures bound with the same cognate ligand and the active site residues in the corresponding site were employed for docking analysis. Docking analysis was done with the andrographolide molecule within the active site of the selected protein structures using GOLD software, and the interactions were analysed. The ligand binding sites were extracted using an in house written Perl script from hydrogen added PDB atom file. The atom numbers for the extracted binding sites were taken and were provided as input for GOLD calculation. Default genetic algorithm (GA) settings that ensure 100% search efficiency were used for docking. An early termination of the number of GA runs was allowed when the RMSDs of the top three GA solutions were within 1.5°A. The best pose of the docked ligand was selected based on CHEMPLP score [16].

2.6. Molecular simulation

Molecular Dynamics (MD) simulations were performed for ICDH and ACC in complex with andrographolide. The Amber ff12SB force field was applied to the protein structure [16]. The topology and parameter files were generated using the tLEAP program [17]. The MD simulation was performed using AM BER 12. The protein structure complexes of ICDH and ACC were surrounded by rectangular periodic box of TIP3P water molecules with a margin of 10.0°A. Na + ions were added to the system to neutralize it. Prior to MD, 1500 steps of steepest-descent minimization and 1000 steps of conjugated gradient minimization were applied to the solvent and the entire model system, respectively. The system was heated from 0 to 300 K gradually over 200 ps (picoseconds) using NVT (constant volume and normal temperature) conditions and then simulations were carried out under NPT conditions at 1 atm pressure for another 200 ps. MD simulation was finally performed for 10 ns at 1 atm and 300 K under the NPT ensemble with a time step of 2 fs (femtoseconds). The temperature was controlled using Langevin dynamics and simulations were run using periodic boundary conditions. The PTRAJ module of AMBER package was used for analyzing the trajectories from MD simulation [18].

2.7. Identification of compounds from A. paniculata that can serve as ideal leads for drug development against tuberculosis (TB)

A. paniculata was screened for antimycobacterial activity against the standard reference strain and two clinical isolates of *M. tuberculosis* (Table 1). Based on the results of LRP assay- the methanolic extract of *A. paniculata* showed maximum antimycobacterial activity against H37Rv, clinical isolate resistant to first line drugs and the drug sensitive clinical isolate at 250 μg/ml. The LRP assay has the advantage of being simpler, faster and less laborious. Natural products from various sources like plants and microorganisms have been screened for antimycobacterial activity using the LRP assay [19,20]. The methanolic extract of *A. paniculata* was selected for further isolation and characterization of active anti-TB molecule. Fractions were isolated and bioassay of isolated fractions was per-

Table 1
Percentage reduction in RLU by *A. paniculata* against *M. tuberculosis* H37Rv and a drug sensitive and MDR clinical isolates.

Strains	*n*-Hexane extract		Methanol extract	
	250 μg/ml	500 μg/ml	250 μg/ml	500 μg/ml
M. tuberculosis H37Rv (Standard strain)	42.99	61.45	72.83	90.77
Sensitive (Sensitive to streptomycin, isoniazid, rifampicin, ethambutol))	40.14	60.66	76.61	93.29
MDR (Resistant to streptomycin, isoniazid, rifampicin, ethambutol)	41.54	63.02	75.68	89.71

Table 2
Percentage reduction in RLU by different fractions of *A. paniculata* against *M. tuberculosis* H_{37}RV, and clinical isolates (both drug sensitive and drug resistant).

Fraction Name	H_{37}Rv (Standard strain)		Clinical isolates sensitive to SHRE*		Clincal isolates resistant to SHRE*	
	250 μg/ml	500 μg/ml	250 μg/ml	500 μg/ml	250 μg/ml	500 μg/ml
FR – I	18.44 ± 5.45^{c}	35.26 ± 9.54^{d}	18.78 ± 2.726^{d}	24.98 ± 2.72^{d}	11.88 ± 8.18^{e}	18.85 ± 2.73^{d}
FR – II	37.99 ± 2.72^{b}	36.99 ± 2.73^{d}	30.73 ± 5.453^{bcd}	42.57 ± 5.43^{cd}	21.71 ± 0.27^{de}	27.65 ± 1.09^{d}
FR – III	47.71 ± 0.00^{b}	59.19 ± 5.45^{bc}	41.83 ± 2.726^{bc}	56.61 ± 5.45^{bc}	27.65 ± 1.09^{cd}	39.34 ± 0.27^{c}
FR – IV	78.49 ± 5.45^{a}	94.12 ± 2.73^{a}	74.42 ± 2.726^{a}	90.42 ± 2.72^{a}	79.34 ± 1.09^{a}	93.04 ± 0.27^{a}
FR – V	46.97 ± 8.17^{b}	68.09 ± 9.22^{b}	51.97 ± 5.453^{b}	63.84 ± 1.09^{b}	48.55 ± 2.73^{b}	56.61 ± 5.45^{b}
FR – VI	$35.48 \pm 2.72b^{c}$	41.90 ± 2.73^{cd}	30.51 ± 8.179^{cd}	39.90 ± 5.45^{cd}	37.75 ± 2.72^{bc}	50.79 ± 1.09^{b}

Values represent mean % reduction in RLU ± SD of three replicates; Means within a column followed by the same letters are not significantly different by Tukey's test at $p = 0.05$.
*SHRE: S–streptomycin, H–isoniazid, R–rifampicin, E–ethambutol.

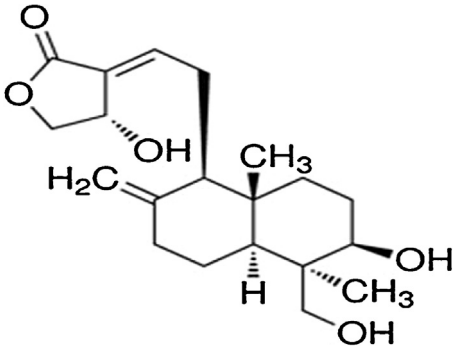

Fig. 2. The chemical structure of the isolated andrographolide molecule from *Andrographis paniculata.*

formed against the clinical isolates (MDR and drug sensitive) as well as the standard strain of *M. tuberculosis,* H_{37}Rv, at two concentrations (250 and 500 μg/ml) using LRP assay in order to identify the potent fractions.

Anti-tubercular activity of the six fractions (Fr 1–Fr 6) eluted from column chromatography on *M. tuberculosis* strains is shown in Table 2. Among the six fractions tested, fraction 4 showed significant activity against *M. tuberculosis* at a concentration of 250 μg/ml. Fractions three (FR-3) and five (FR-5) had moderate activity at a higher concentration of 500 μg/ml.

Further purification of the active fraction 4 was accomplished using TLC, and this was confirmed by HPTLC. The HPTLC scanning profile revealed that the active compound showed a single peak with high intensity, while the crude extract track showed six peaks (Fig. 1A and B). Syed et al. [21], justified the use of HPTLC for checking the purity of the isolated compound and estimation of active constituents with reasonable accuracy in a short time. The active fraction was subjected to spectral analyses (UV, FT-IR and NMR) to further characterize the compound.

Based on the above results and other spectral data from ^{1}H, ^{13}C–NMR, the structure of the active compound was determined to be *Andrographolide* (Fig. 2). Its molecular formula is $C_{20}H_{30}O_{5}$, molecular wt. is 350.4492 and melting point is 228–230 °C. The spectral data obtained was identical to that reported by Siripong et al. [22] and Kulyal et al. [23].

Recently, other investigators studied the cytotoxic potential of andrographolide on *M. microti* [24] and *M. bovis* [25], and reported that it was non-cytotoxic at concentrations at which more than 96% inhibition was observed.

Andrographolide has been reported to have several targets in humans for various diseases such as cancer, diabetes, etc. Some of the targets of andrographolide in human for various types of cancer include cAMP-dependant protein kinase, Human AbI kinase, PI3 kinase, epidermal growth factor receptor, etc. [26]. In order to identify the probable target protein for andrographolide in *M. tuberculosis,* docking analysis was performed with known drug targets.

2.8. *Identification of potential* M. tuberculosis *protein targets for Andrographolide using docking analysis*

Three dimensional structures were collected for all known drug targets of *M. tuberculosis* from *Mycobacterium tuberculosis* Structural Database (MtbSD) [27] and from the recent publications on tuberculosis drug targets [28]. The structures for the reported drug targets were downloaded from MtbSD and PDB databases (Table 3). The PDB file was checked for alternative side chain conformation and was corrected using Discovery Studio V 2.0. The protein structure of the selected drug targets were protonated using the GOLD utility programs. Further, the protein structure from the list of available structures for the individual gene, with no mutations for the selected drug targets was selected based on the alignment between sequence from Swissprot and PDB available in MtbSD database. The protonated structure of the selected drug targets having no mutations, based on the alignment for these proteins present in MtbSD, was used for docking.

The docking score of andrographolide against 22 drug targets listed in (Table 4) reveals that ICDH (RV339C) and AAC (RV0262C) had the highest gold score of 60.98 and 68.01 respectively. However for the other targets, the binding score ranged from 14.63 to 59.05. Based on the above data ICDH and AAC were selected for further analysis. The binding interaction of the docked andrographolide within the active sites of ICDH and AAC is shown in Fig. 3A and B.

2.9. *Stability of the andrographolide target complex by MD simulation*

Proteins are dynamic macromolecules in physiological conditions interacting with the medium which generally is composed of water. The dynamic process can affect the conformation of both the protein and its bound ligands. Dynamic simulation is a widely

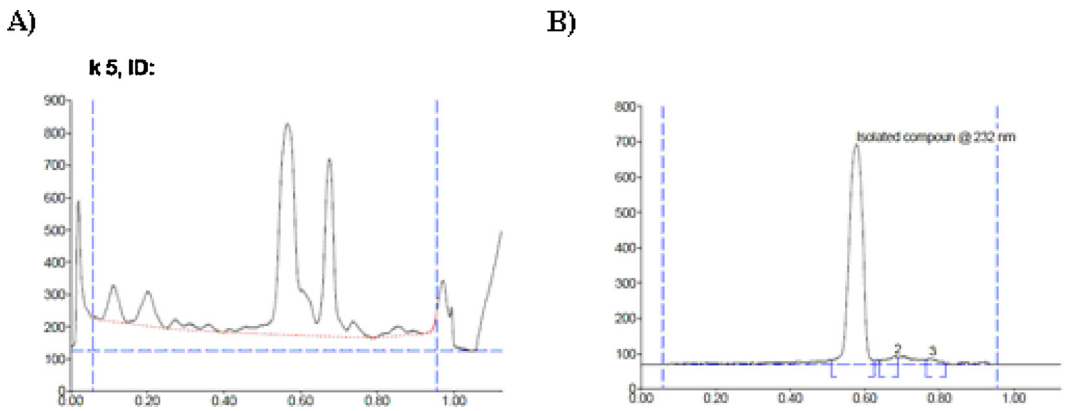

Fig. 1. HPTLC profile of *Andrographis paniculata.* (A) Tracks showing active crude extract. (B) Single track showing identified active fraction.

Table 3
List of the selected drug targets from the genome of *M. tuberculosis.*

Rv number	PDB ID	Macromolecule name
Rv3339c	4HCX	Isocitrate Dehydrogenase-1 (ICDH)
Rv0467	1F8M	ISOCITRATE LYASE
Rv2429	1KNC	AhpD protein
Rv3240c	1NKT	Preprotein translocase secA 1 subunit
Rv1483	1UZL	3-OXOACYL-[ACYL-CARRIER PROTEIN] REDUCTASE
Rv3423c	1XFC	Alanine racemase
Rv2626c	1XKF	hypothetical protein RV2626C
Rv1908c	2CCA	PEROXIDASE/CATALASE T
Rv0014c	2FUM	Probable serine/threonine-protein kinase pknB
Rv0410c	2PZI	Probable serine/threonine-protein kinase pknG
Rv1484	2 × 23	ENOYL-[ACYL-CARRIER-PROTEIN] REDUCTASE [NADH]
Rv3133c	3C3W	TWO COMPONENT TRANSCRIPTIONAL REGULATORY PROTEIN DEVR
Rv2623	3CIS	Uncharacterized protein
Rv1009	3E05	Precorrin-6Y C5,15-methyltransferase (Decarboxylating)
Rv0462	3II4	Dihydrolipoyl dehydrogenase
Rv0262c	1M4I	Aminoglycoside 2'-N-acetyltransferase (AAC)
Rv3913	2A87	Thioredoxin reductase
Rv2069	2O7G	ECF RNA polymerase sigma factor SigC
Rv0533c	2QX1	3-oxoacyl-[acyl-carrier-protein] synthase 3
Rv2245	2WGE	3-oxoacyl-[acyl-carrier protein] synthase 1 KasA (beta-ketoacyl-ACP synthase)
Rv3793	3PTY	Integral membrane indolylacetylinositol arabinosyltransferase EmbC
Rv2981c	3LWB	Probable D-alanine–D-alanine ligase DdlA

Table 4
The docking score of andrographolide using GOLD software against the 22 selected drug targets of MTB.

Rv number	PDB ID	Gold score	Macromolecule name
Rv3339c	4HCX	60.98	Isocitrate Dehydrogenase-1 (ICDH)
Rv0467	1F8M	NIL	Isocitrate lyase
Rv2429	1KNC	28.89	AhpD protein
Rv3240c	1NKT	52.7	Preprotein translocase secA 1 subunit
Rv1483	1UZL	14.63	3-Oxoacyl-[Acyl-Carrier Protein] Reductase
Rv3423c	1XFC	39.36	Alanine racemase
Rv2626c	1XKF	NIL	hypothetical protein RV2626C
Rv1908c	2CCA	47.75	Peroxidase / Catalase T
Rv0014c	2FUM	46.21	Probable serine/threonine-protein kinase pknB
Rv0410c	2PZI	48.18	Probable serine/threonine-protein kinase pknG
Rv1484	2X23	54.1	Enoyl-[Acyl-Carrier-Protein] Reductase [NADH]
Rv3133c	3C3W	30.49	Two component transcriptional regulatory protein DEVR
Rv2623	3CIS	39.76	Uncharacterized protein
Rv1009	3E05	37.46	Precorrin-6Y C5,15-methyltransferase (Decarboxylating)
Rv0462	3II4	46.59	Dihydrolipoyl dehydrogenase
Rv0262c	1M4I	68.01	Aminoglycoside 2'-N-acetyltransferase (AAC)
Rv3913	2A87	55.01	Thioredoxin reductase
Rv2069	2O7G	28.31	ECF RNA polymerase sigma factor SigC
Rv0533c	2QX1	59.05	3-oxoacyl-[acyl-carrier-protein] synthase 3
Rv2245	2WGE	NIL	3-oxoacyl-[acyl-carrier protein] synthase 1 KasA (beta-ketoacyl-ACP synthase)
Rv3793	3PTY	58.31	Integral membrane indolylacetylinositol arabinosyltransferase EmbC
Rv2981c	3LWB	NIL	Probable D-alanine–D-alanine ligase DdlA

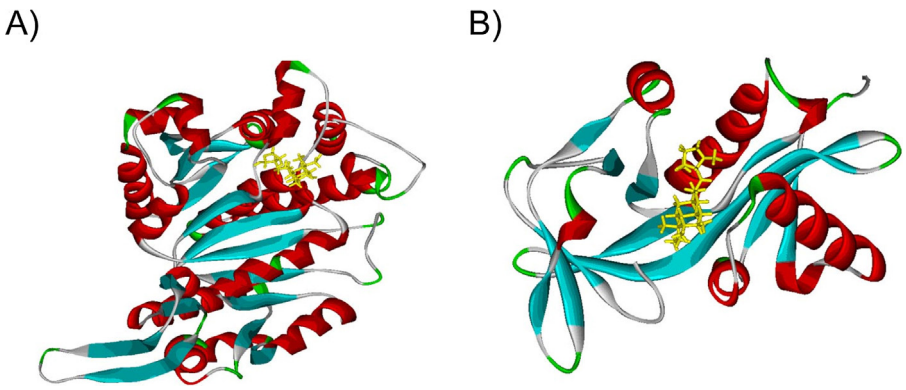

Fig. 3. Docking pose of andrographolide. (For interpretation of the references to colour in this figure legend, the reader is referred to the web version of this article.)
(A) The crystal structure of Isocitrate Dehydrogenase-1 (PDB ID 4HCX) docked with andrographolide. The docked andrographolide is represented in stick form (yellow). (B) The crystal structure of Aminoglycoside 2'-*N*-acetyltransferase (PDB ID 1M4I) docked with andrographolide. The andrographolide molecule is represented in stick form (yellow).

used method to obtain information on the time evolution of conformations of proteins and other biological macromolecules [29]. To further define the stability of the andrographolide bound structures of 4HCX and 1M4I, MD simulation was performed. MD simulation was done for 10 ns for the andrographolide docked structures of 4HCX and 1M4I to analyze the stability of ligand-protein complex.

After 10 ns of MD simulation, the potential energy along the trajectory was plotted. According to the RMSD plot calculated from the MD simulation of the protein ligand complexes, the presence of the docked andrographolide within the active site had stabilized for 1M4I. However, the presence of andrographolide within the active site of 4HCX resulted in large fluctuations, implying instability of the bound andrographolide within this complex (Fig. 4). Interestingly, the trajectory analysis revealed that the andrographolide exited the binding pocket of 4HCX after 10 ns of simulation. Garima Tiwari and Debasisa Mohanty [30–32] have reported that the deviation of the bound ligand from the binding pocket during MD simulations would indicate low binding affinity of the ligand (28). Thus, our results indicate that 4HCX has low binding affinity to andrographolide. This justifies that ACC (PDB ID 1M4I) could be the most probable target for andrographolide. Further, for 1M4I, the andrographolide was observed to be well within the active range after 10 ns of molecular simulations. This also justifies that ACC (PDB ID 1M4I) could be the probable target for andrographolide.

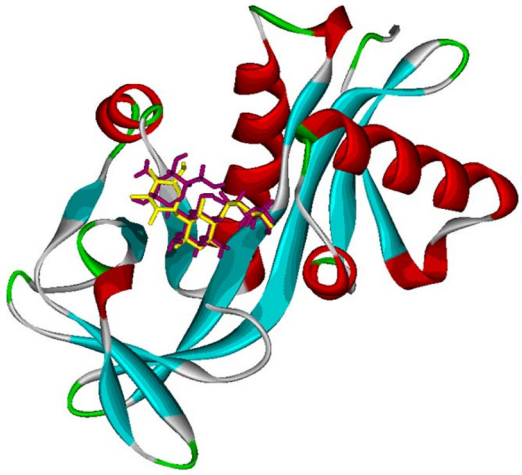

Fig. 5. Overlay of the docked and crystal structure of 1M4I in complex with kanamycin. (For interpretation of the references to colour in this figure legend, the reader is referred to the web version of this article.)
Structural **s**uperimposition between the docking result and the crystal structure of 1M4I in complex with kanamycin. The docked kanamycin is colored in purple whereas the kanamycin present in the crystal structure is colored in yellow.

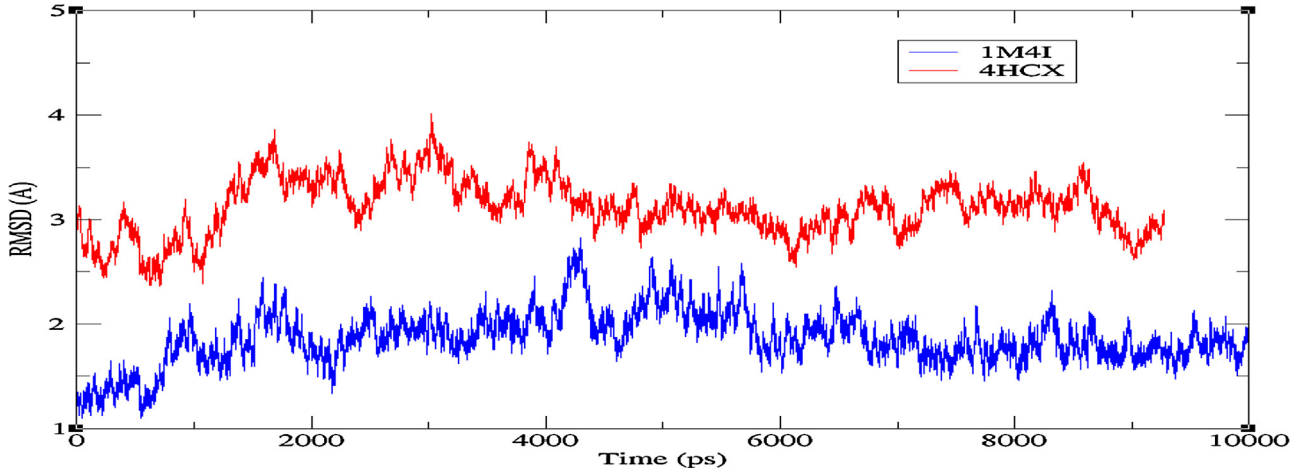

Fig. 4. RMSD plot in MD simulation. (For interpretation of the references to colour in this figure legend, the reader is referred to the web version of this article.)
The RMSD values using the backbone atoms of the crystal structures of 4HCX (red line) and 1M4I (blue line) docked with andrographolide relative to their starting structure during molecular simulation.

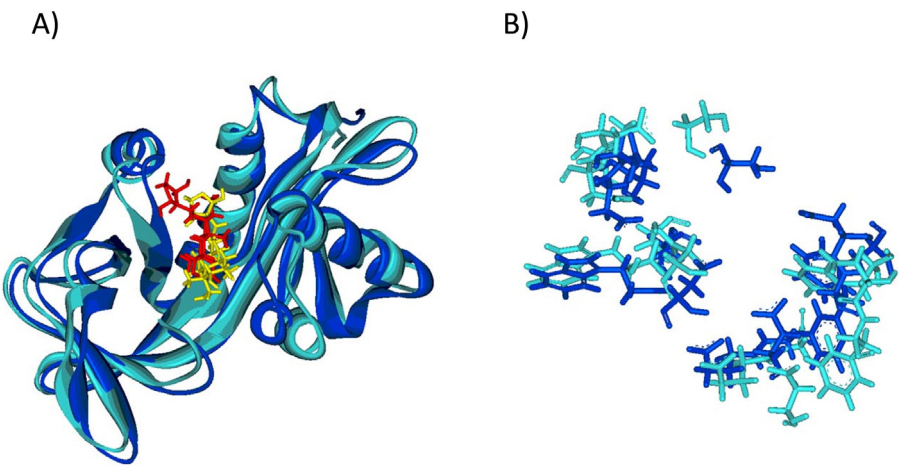

Fig. 6. Comparison of 1M4I - and rographolide complex before and after MD. (For interpretation of the references to colour in this figure legend, the reader is referred to the web version of this article.)
(A) Structural superimposition of 1M4I docked complex of andrographolide before (blue) and after (cyan) simulation. The ligand is seen repositioning itself within the active site of 1M4I after simulation. (B) Structural overlap of the active site residues of 1M4I structure before and after MD simulation. Blue colour represents the initial structure and cyan colour represents the structure after simulation.

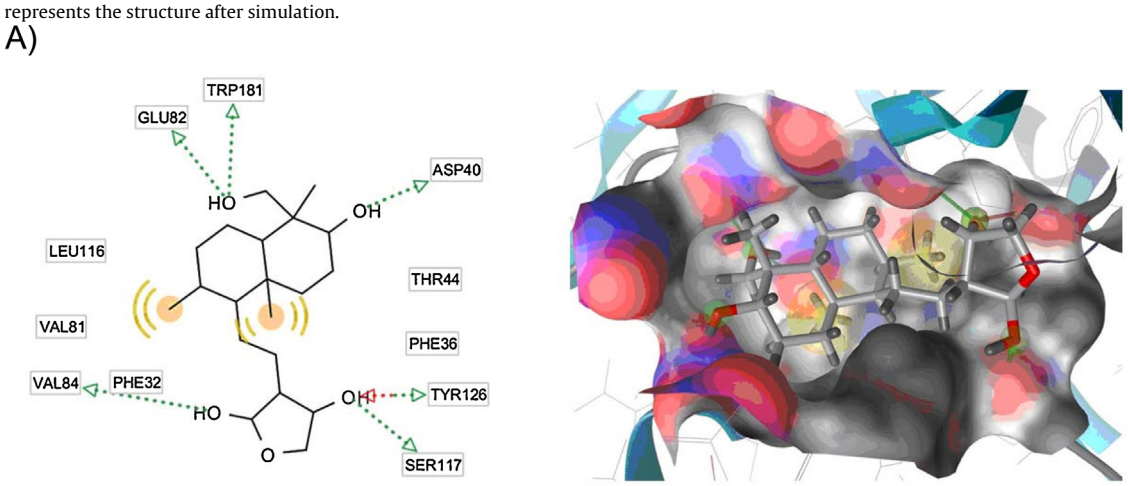

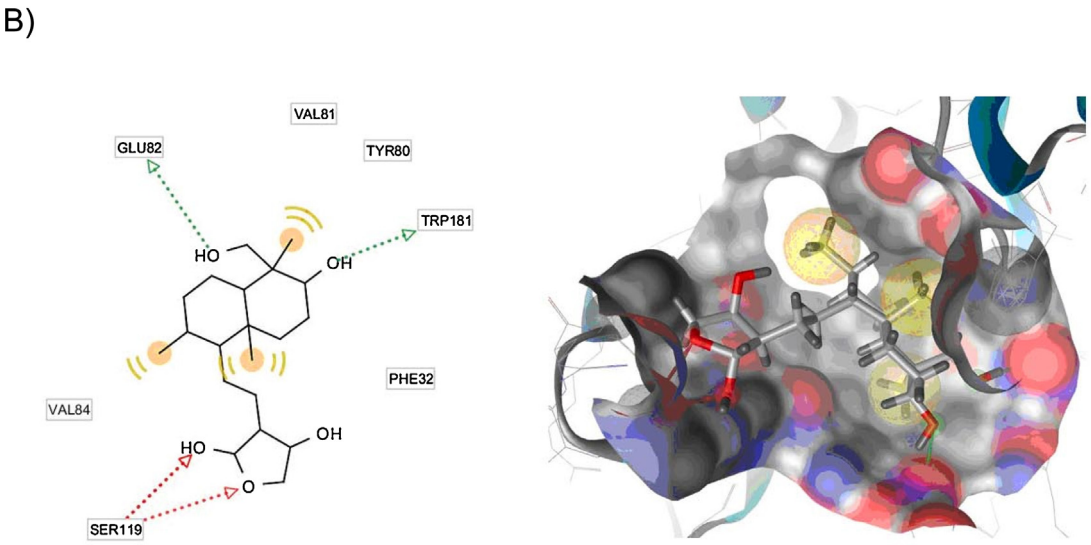

Fig. 7. Binding of andrographolide within the active site of 1M4I. (For interpretation of the references to colour in this figure legend, the reader is referred to the web version of this article.)
(A) Interaction of amino acids with andrographolide before MD simulation and its pose within the active site of 1M4I. (B) Interaction of amino acids with andrographolide after MD simulation and its pose within the active site of 1M4I. The hydrogen bond donor, hydrogen bond acceptor and hydrophobic interactions are shown as green dotted line, red dotted line and yellow respectively. The active site surface is colored by electrostatic properties.

Aminoglycoside 2′-*N*-acetyltransferase (AAC) is a 181 amino acid long protein that confers resistance to aminoglycosides. The crystal structure of AAC (1M4I) [33] is available as a complex with Kanamycin. Based on docking results, AAC was identified and predicted as a potential target protein for andrographolide. Andrographolide had the highest binding affinity to AAC protein than to other target proteins based on GOLD score. Further, comparing the binding affinity of andrographolide and kanamycin, AAC is predicted to have a better binding affinity to andrographolide (68.01) than kanamycin (61.07). The docked pose of kanamycin and crystal structure of 1M4I in complex with kanamycin is shown in Fig. 5. The top ranked pose of andrographolide in the active site of AAC was found to interact with most of the key residues *viz.* Val 84, Asp 40, Glu 82, Ser 117, Trp 181, Leu 16, Thr 44, Val 81, Phe 36, Phe 32, and Tyr 126 of AAC protein that interacted with kanamycin.

Superimposition of Cα atoms of 1M4I before and after MD simulation revealed an RMSD of 1.8A (Fig. 6A). Comparison of the active site residues of the superimposed initial and simulated structures revealed conformational changes at these residues (Fig. 6B). The MD simulation suggests that the active site residues of 1M4I are flexible, thus establishing the fact that reorganization of the active site residues is necessary to bring about a change in its shape to achieve complementarity with the ligand structure. Analysis of the interacting residues with andrographolide (Fig. 7A and B) shows that five residues, *viz.* Trp 181, Val 84, Phe 32, Glu 82 and Val 81, maintained their interaction with andrographolide inspite of the conformational changes induced due to simulation.

Binding free energy of andrographolide to 1M4I was computed from the MD trajectories using MM-PBSA. It was earlier reported that when flexibilities are introduced into the protein and ligand, the computed binding energy values show better correlation with experimental results [34]. Thus, the MM- BSA binding free energy value, $\Delta G_{bind} = -12.27$calculated for andrographolide within the binding site of 1M4I after MD simulation revealed that 1M4I could be a probable target protein for andrographolide.

3. Conclusions

The present study reinvestigated the importance of traditional phyto–medicines for the discovery of new molecules effective against TB. Andrographolide isolated from *A. paniculata* was found to demonstrate potent antimycobacterial activity. Docking analysis predicted both ICDH and AAC as potential targets of andrographolide in *M. tuberculosis.* Molecular simulation revealed that ICDH had a low binding affinity to andrographolide. However, for AAC, the andrographolide was observed to be well within the active range after 10 ns of molecular simulations. This implies that ACC (PDB ID 1M4I) could be the most probable target for andrographolide. However, further *in vivo* studies and clinical trials would be needed to justify the potential of this compound as an antimyobacterial agent.

Acknowledgements

The authors wish to acknowledge Dr. Soumya Swaminathan, Director, National Institute for Research in Tuberculosis (NIRT) for providing facilities to carry out this work. We also thank Mr. R. Senthil Nathan, National Institute for Research in Tuberculosis (NIRT), for editing figures.

References

[1] S.K. Sharma, A. Mohan, Tuberculosis From an incurable scourge to a curable disease—journey over a millennium, Indian J. Med. Res. 137 (March (3)) (2013) 455–493.
[2] World Health Organisation 2014. Global report, 2014. WHO/HTM/TB/2014.08.
[3] Centers for Disease Control and Prevention. Emergence of *Mycobacterium tuberculosis* with extensive resistance to second-line drugs–worldwide, 2000–2004. MMWR Morb Mortal Wkly Rep 2006; 55:301-5.
[4] N.S. Shah, A. Wright, G.H. Bai, L. Barrera, F. Boulahbal, N. Martin-Casabona, F. Drobniewski, C. Gilpin, M. Havelkova, R. Lepe, R. Lumb, B. Metchock, F. Portaels, M.F. Rodrigues, S. Rusch-Gerdes, A. Van Deun, V. Vincent, K. Laserson, C. Wells, J.P. Cegielski, Worldwide emergence of extensively drug-resistant tuberculosis, Emerg. Infect. Dis. 13 (2007) 380–387.
[5] J.H. Zhang, T.D. Chung, K.R. Oldenburg, A simple statistical parameter for use in evaluation and validation of high throughput screening assays, J. Biomol. Screening 4 (1999) 67–73.
[6] D.J. Newman, G.M. Cragg, Natural products as sources of new drugs over the last 25 years, J. Nat. Prod. 70 (2007) 461–477.
[7] J.B. Calixto, Twenty-five years of research on medicinal plants in Latin America: a personal view, J. Ethnopharmacol. 100 (2005) 131–134.
[8] B. Patawardhan, Drug discovery and development: Traditional medicine and ethnopharmacology, New India Publishing Agency, New Delhi, 2007.
[9] R. Gautam, A. Saklani, S.M. Jachak, Indian medicinal plants as a source of antimycobacterial agents, J. Ethnopharmacol. 110 (2007) 200–234.
[10] K.M. Nadkarni, Indian Meteria Medica, Popular Prakashan, Bombay, India, 2005.
[11] P.K. Mukherjee, Quality Control of Herbal Drugs, Business Horizons Ltd., New Delhi, India, 2002.
[12] A.M. Ahmad, A.F. Alkarkhi, S. Hena, B.M. Siddique, K.W. Dur, Optimization of Soxhlet extraction of Herba Leonuri using factorial design of experiment, Int. J. Chem. 2 (2010) 198–205.
[13] P.M. Sivakumar, S. Prabhu Seenivasan, V. Kumar, M. Doble, Novel 1,3,5-triphenyl-2-pyrazolines as anti-infective agents, Bioorg. Med. Chem. Lett. 20 (2015) 3169–3172.
[14] S. Kandasamy, S. Hassan, R. Gopalaswamy, S. Narayanan, Homology modelling, docking, pharmacophore and site directed mutagenesis analysis to identify the critical amino acid residue of PknI from *Mycobacterium tuberculosis*, J. Mol. Graph. 52 (2015) 11–19.
[15] D.L. Wheeler, T. Barrett, D.A. Benson, S.H. Bryant, K. Canese, V. Chetvernin, D.M. Church, M. DiCuccio, R. Edgar, S. Federhen, L.Y. Geer, W. Helmberg, Y. Kapustin, D.L. Kenton, O. Khovayko, D.J. Lipman, T.L. Madden, D.R. Maglott, J. Ostell, K.D. Pruitt, G.D. Schuler, L.M. Schriml, E. Sequeira, S.T. Sherry, K. Sirotkin, A. Souvorov, G. Starchenko, T.O. Suzek, R. Tatusov, T.A. Tatusova, L. Wagner, E. Yaschenko, Database resources of the National Center for Biotechnology Information, Nucleic Acids Res. 34 (2006) D173–D180 (Database issue).
[16] E. Kellenberger, J. Rodrigo, P. Muller, D. Rognan, Comparative evaluation of eight docking tools for docking and virtual screening accuracy, Proteins 57 (2004) 225–242.
[17] Y. Duan, C. Wu, S. Chowdhury, M.C. Lee, G. Xiong, W. Zhang, R. Yang, P. Cieplak, R. Luo, T. Lee, J. Caldwell, J. Wang, P. Kollman, A point-charge force field for molecular mechanics simulations of proteins based on condensed-phase quantum mechanical calculations, J. Comput. Chem. 24 (2003) 1999–2012.
[18] D.S. Cerutti, R. Duke, P.L. Freddolino, H. Fan, T.P. Lybrand, Vulnerability in popular molecular dynamics packages concerning langevin and andersen dynamics, J. Chem. Theory Comput. 4 (2008) 1669–1680.
[19] K. Wittayanarakul, S. Hannongbua, M. Feig, Accurate prediction of protonation state as a prerequisite for reliable–B (GB) SA binding free energy calculations of V–1 protease inhibitors, J. Comput. Chem. 29 (5) (2007) 673–685.
[20] Prabuseenivasan S, Kumar V. Rapid screening of selected plant essential oils against *Mycobacterium tuberculosis* using Luciferase Reporter Phage (LRP) assay.2007; p. 107-114. *In* R. Balagurunathan and M. Radhakrishnan (ed.), Proceedings of the National Seminar on Microbial Biotechnology, Sri Sankara Arts & Science College, Kanchipuram.
[21] M.S. Radhakrishnan, R. Suganya, R. Balagurunathan, K. Vanaja, Preliminary screening for antibacterial and antimycobacterial activity of actinomycetes from less explored ecosystems, World J. Microbiol. Biotech. 26 (2010) 561–566.
[22] M.H. Syed, A. Yasmeen, M.S. Hussain, N.S. Subramanian, M. Ramadevi, Preliminary phytochemical screening and HPTLC fingerprinting of leaf extracts of *Pisonea aculeata*, J. Pharmacog. Phytochem. 2 (1) (2013) 36–42.
[23] P. Siripong, B. Kongkathip, K. Preechanukool, P. Picha, K. Tunsuwan, W.C. Taylor, Cytotoxic diterpenoid constituents from *A. paniculata* Nees leaves, J. Sci. Soc. Thailand 18 (1992) 187–194.
[24] P. Kulyal, U.K. Tiwari, A. Shukla, A.k. Gaur, Chemical constituent isolated from *A. paniculata*, Indian J. Chem. (2010) 356–359.
[25] A. Shrivastava, H.K. Garg, Cytotoxic potential of andrographolide against bovine tuberculosis, IOSR J. Pharm. Biol. Sci. 8 (5) (2013) 01–04.
[26] A., Shrivastava, H.K., Garg. Effect of Andrographolide on Proliferation of Mycobacterium canetti. International Journal for Pharmaceutical Research Scholars 2013; V-(3), I-1.
[27] K.M. Sharmila, S. Subburathinam Aishwarya, A. Margret, In-silico analysis of andrographolide against cancer, Int. J. Pharm. Sci. Drug Res. 5 (2) (2013) 56–61.
[28] S. Hassan, P. Logambiga, A.M. Raman, T.K. Subazini, V. Kumaraswami, L.E. Hanna, MtbSD–a comprehensive structural database for *Mycobacterium tuberculosis*, Tuberculosis 91 (2015) 556–562.
[29] B.K. Chung, T. Dick, D.Y. Lee, In silico analyses for the discovery of tuberculosis drug targets, J. Antimicrob. Chemother. 68 (2015) 2701–2709.
[30] P. Kamsri, N. Koohatammakun, A. Srisupan, P. Meewong, A. Punkvang, P. Saparpakorn, S. Hannongbua, P. Wolschann, S. Prueksaaroon, U.

Leartsakulpanich, P. Pungpo, Rational design of InhA inhibitors in the class of diphenyl ether derivatives as potential anti-tubercular agents using molecular dynamics simulations, SAR QSAR Environ. Res. 25 (6) (2014) 473–488.
[31] W.F. De Azevedo Jr., Molecular dynamics simulations of protein targets identified in *Mycobacterium tuberculosis*, Curr Med Chem. 18 (9) (2011) 1353–1366.
[32] T.E. Cheatham 3rd, P.A. Kollman, Molecular dynamics simulation of nucleic acids, Annu. Rev. Phys. Chem. 51 (2000) 435–471.
[33] M.W. Vetting, S.S. Hegde, F. Javid-Majd, J.S. Blanchard, S.L. Roderick, Aminoglycoside 2′-*N*-acetyltransferase from *Mycobacterium tuberculosis* in complex with coenzyme A and aminoglycoside substrates, Nat. Struct. Biol. 9 (9) (2002) 653–658.
[34] G. Tiwari, D. Mohanty, An in silico analysis of the binding modes and binding affinities of small molecule modulators of PDZ-peptide interactions, PLoS One 8 (2013) e71340.